AN EULERIAN ALGORITHM FOR ANALYZING FLUID–STRUCTURE INTERACTION IN THE FAST REACTOR CONTAINMENT

C. Y. WANG, Y. W. CHANG, S. H. FISTEDIS

Reactor Analysis and Safety Division, Argonne National Laboratory
9700 South Cass Avenue, Argonne, Illinois 60439, U.S.A.

SUMMARY

The response of the primary containment to an HCDA depends on a number of factors, including the HCDA energy source, propagation of the pressure waves, and interaction of fluid with internal structural components, especially for those adjacent to the core. In the past decade, substantial amount of research effort has been devoted to the development of computer programs for performing numerical analysis on the fluid-structure interactions. Although the Lagrangian technique has been widely adopted by most investigators, it has difficulties in handling (1) sliding boundary conditions at interfaces of fluids and reactor internals, and (2) fluid motions at geometry discontinuities, such as sharp corners and irregularities. Also, the inability of the method to treat excessive distortions has further prevented it from applying to the problems involving bubble expansion and sodium spillage.

To overcome these difficulties, this paper presents an algorithm for analyzing the coupled fluid-structure problems in the LMFBR consisting of various internals and primary vessel. The aim is at the development of a generalized Eulerian hydrodynamic scheme, which can be used to link together the ICE technique with the finite-element structural dynamics method to provide sliding capability at interface, modeling of perforated structure, and analyses of fluid motions at the geometry discontinuity. Since the finite-element method has been already well developed, the work described herein thus will concentrate on the fluid-structure interaction.

The algorithm uses the Eulerian description in the hydrodynamic formulation principally because it has the deciding advantage of treating excessive distortion. It employs the implicit temporal integration scheme to solve the nonlinear, time-dependent equations of fluid mechanics. This scheme not only ensures computational stability, but also eases the Couriant condition on the time step. Furthermore, the Implicit treatment of pressure and velocity fields allows the presence of all flow-speed regimes. Hence, the algorithm is applicable to any degree of excursion.

In the analysis, a special equation for the pressure adjacent to the structure is derived, which allows us to adjust the pressure proportional to the actual mass flux across the boundary. This equation, in conjunction with the Poisson equation for the pressure in the fluid region, is solved iteratively. The convergence is attained when boundary conditions at all interfaces are rigorously satisfied. In other words, for the deformable structure without openings, the iteration is continued until the fluid slides tangentially. Whereas for the perforated structure, the procedure is repeated until the uniform mass flux across the boundary equals to the total mass flux through the openings.

Two sample problems are given, concerning wave propagation in a typical LMFBR which consists of radial shield, core barrel, core-support structure, and the primary vessel. The first problem computes the deformation histories of various structure components. The second problem examines the influence of core-support structure openings on the pressure loading in the reactor lower plenum. Results reveal that this algorithm can offer a stable and accurate solution, and is particularly suitable for the coupled fluid-structure problems possessing strong material distortion.

1. Introduction

One important concern in the safety analysis of LMFBRs is the dynamic response of the primary containment generated by the fluid-structure interaction during an HCDA. The analysis is highly complex since it involves calculations of nonlinear fluid transient, fluid-structure interaction, and the resulting structure response. At the present time there are several techniques available for such analysis, but to the authors' knowledge no effective method has been developed which can rigorously treat the fluid-structure interaction for the excursions encompassing bubble migration and sodium spillage.

With an attempt to solve the coupled fluid-structure problem, substantial research effort has been devoted in the application of the existing hydrodynamic techniques for performing the numerical analysis of the fluid-structure interaction. Among all the techniques, the Lagrangian finite-difference method has been widely adopted by many investigators. This method provides great resolution at the early stage of excursion, but cannot handle strong material distortion such as bubble contraction and sodium spillage. Also, it has difficulties of treating the sliding boundary condition at interface of fluids and reactor internals, as well as handling the fluid motion at geometrical discontinuities, such as sharp corners and other irregularities.

On the other hand, the Eulerian hydrodynamic methods [1,2] are excellent to treat distortion. However, these methods lack the capability for treating the time-dependent irregular cells created by the movement of the structure with respect to the fixed Eulerian coordinates. Thus, the engineering applications have been limited by the requirement that the external boundary and internal structure must be placed on the Eulerian grid lines.

To overcome the difficulties of both Lagrangian and Eulerian methods as mentioned above, this paper describes an algorithm for analyzing the fluid-structure interactions in the LMFBR, consisting of complicated structures such as the radial shield, core barrel, core-support structure, and the primary containment. The emphasis is on the development of a generalized hydrodynamic scheme to treat the irregular cell, and to provide sliding capability at the interface and modeling of the perforated structure, as well as analysis of fluid motion at the geometry discontinuity. The developed scheme enables the implicit Eulerian hydrodynamic techniques to be coupled with any structure-dynamics program. Presently, this generalized scheme has been integrated with the ICECO [3,4] and WHAM [5] programs for investigating the coupled fluid-structure interaction in an excursion that may involve excessive material distortion.

In this paper, an analytical development for treating fluid-structure interaction is presented. A relaxation equation for pressure in the region containing either nonperforated or perforated structure is derived. This equation, in conjunction with the Poisson equation governing the pressure in the fluid region, is to be solved iteratively. Convergence is attained when boundary conditions at all interfaces are satisfied. To illustrate the analysis two sample problems are given. The results are discussed in detail.

2. Description of the Numerical Algorithm

2.1 The Governing Hydrodynamic Difference Equation

The partial differential equations used in the method are the continuum-mechanics conservation equations of mass, momentum, and energy, and the equation of state of the media. Only axial symmetric flow is considered, and no external energy source is assumed to exist inside the fluid region. The Eulerian coordinates system is used in the formulation, so that the algorithm can be applied to excursions involving arbitary material distortions.

As suggested by Harlow and Amsden [1], the algorithm employs an implicit difference scheme to the set of nonlinear hydrodynamic equations. The convective terms in the mass equation and the pressure gradients in the momentum equations are evaluated at an advanced time. To simplify the description of the method, the detailed derivations of finite-difference expressions of mass and momentum equations will not be presented here, but are given in refs. [1] and [3]. Thus, eliminating the mass flux between the mass and momentum equations, in conjunction with the equation of state relating the advanced-time pressure and densities, results in a Poisson's equation governing the advanced-time pressure:

$$p_{i,j}^{n+1}\left[\frac{1}{c_{i,j}^{n}} + 2\delta t^2\left(\frac{1}{\delta r^2} + \frac{1}{\delta z^2}\right)\right] = G_{i,j}^{n} + \delta t^2\left[\frac{r_{i-1/2}p_{i-1,j}^{n+1} + r_{i+1/2}p_{i,j-1}^{n+1}}{r_i \delta r^2} + \frac{p_{i,j-1}^{n+1} + p_{i,j+1}^{n+1}}{\delta z^2}\right] \quad (1)$$

where

$$c_{i,j}^{n} = \left(\frac{\partial p}{\partial \rho}\right)_{i,j}^{n}$$

and

$$G_{i,j}^{n} = G(u^n,\ v^n,\ p^n,\ \mu,\ \lambda,\ \delta t,\ \delta r,\ \delta z)$$

is the source term evaluated from previous cycle values, δt is the time step, δr and δz are, respectively, the dimensions of a cell in the radial and axial directions. Also, in Eq. (1) the superscripts n+1 and n denote the (n+1)-th and n-th time cycles; while subscripts i and j indicate spatial values.

It should be mentioned that Eq. (1) is the governing difference equation for the advanced pressure in the fluid region. This equation is expressed in the implicit version. It is a five-point equation that is solved by the iteration technique.

In the iteration process, a much improved formula is used by replacing $(p_{i-1,j}^{n+1})^{h}$ and $(p_{i,j-1}^{n+1})^{h}$ with the latest iterates $(p_{i-1,j}^{n+1})^{h+1}$ and $(p_{i,j-1}^{n+1})^{h+1}$ while sweeping the direction of increasing i and j. This yields

$$(p_{i,j}^{n+1})^{h+1}\left[\frac{1}{c_{i,j}^{n}} + 2\delta t^2\left(\frac{1}{\delta r^2} + \frac{1}{\delta z^2}\right)\right]$$
$$= G_{i,j}^{n} + \delta t^2\left[\frac{r_{i-1/2}(p_{i-1,j}^{n+1})^{h+1} + r_{i+1/2}(p_{i+1,j}^{n+1})^{h}}{r_i \delta r^2} + \frac{(p_{i,j-1}^{n+1})^{h+1} + (p_{i,j+1}^{n+1})^{h}}{\delta z^2}\right], \quad (2)$$

where h and h+1 denote previous and latest iteration, respectively.

2.2 Fluid-structure Interaction

The fluid-structure interaction occurs in the Eulerian cell containing the deformable structure. The hydrodynamic analysis furnishes the structural program with a pressure distribution. The structural program calculates the displacement and velocity of the component, and feeds back this information to the hydrodynamic calculation. Based upon the displacement and velocity of the deformed structure, the fluid particle and structure are appropriately matched together at the interface, where the physical boundary condition should be satisfied. Since the viscosity of liquid is very small, an inviscid boundary condition is thus employed in the algorithm.

Analysis of fluid-structure interaction is very complex. The major difficulty is the treatment of the boundary condition at the interface as the structure is displaced across the fixed Eulerian grids. The analysis is further complicated if the structure possesses certain perforated openings as shown in Fig. 1. One way of dealing with this problem is using the control-volume technique to derive the conservation equations and their difference representation with respect to the partial cell which is actually occupied by the fluid (such as CDEF shown in Fig. 1). However, because the structure component in general moves two-dimensionally, and the shape of the partial cell is highly irregular, the procedure of the control-volume technique is too cumbersome.

As an alternative to the control-volume method, we derive a generalized relaxation equation which is applicable to either the nonperforated or the perforated structure. This equation allows us to adjust the pressure proportional to the actual mass flux across the boundary. If h and h+1 denote the previous and the new iterate, respectively, the equation is

$$p^{h+1}_{k,\ell} = p^{h}_{k,\ell} - \frac{\Delta\tau}{\delta}\left\{\rho(\bar{V}^{h}_{p} - \bar{V}_{b}) \cdot \bar{n} - \theta\right\}_{k,\ell} \tag{3}$$

in which

$$\delta = \min[\delta r, \delta z]$$

and

$$\Delta\tau \leq \delta^2/2\delta t \ .$$

In eq. (3) the subscripts k and ℓ refer to the irregular cell (k,ℓ); $\bar{V}_b$ is the velocity of the structure; $\bar{V}_p$ is the velocity vector of the fluid particle; $\bar{n}$ is the unit normal of the boundary pointing into the fluid.

For the perforated structure, the amount of mass flux, $\theta_{k,\ell}$, through the structure openings can be calculated from

$$\theta_{k,\ell} = (\rho\psi u)_{k,\ell} \tag{4}$$

where ψ is the perforated ratio, defined as the ratio of the flow area to the total area covered by the structure member. The change of the fluid velocity u in the coolant-passage openings can be calculated from

$$\frac{du}{dt} = \frac{P_{k,\ell} - P_{k,\ell-1} - \Delta p}{\rho L} \ , \tag{5}$$

where $P_{k,\ell-1}$ and $P_{k,\ell}$ are the pressures on both sides of the structure, L is the mean length of the coolant passage associated with the corresponding structure member, Δp is the pressure loss due to friction and in certain circumstances can be directly related to $|u|^{1.75}$.[see ref.6].

2.3 Multivalued Field Variable Adjacent to the Internal Structure

Since fluids have different motions on both sides of the internal structure, the field variables such as p,ρ,u, and v in the cell containing structure are assumed to have difference values. For instance, if cell (i,j) contains the core barrel where both sides are submerged in the fluid; then the field variables should have two sets of value. The variables p_ℓ, ρ_ℓ, u_ℓ, and v_ℓ are calculated in such a way that the fluid on the left-hand side of the core barrel slides tangentially. Likewise, p_r, ρ_r, u_r, and v_r are obtained so that the fluid on its right-hand side also moves tangentially. Similarly, field variables

can be obtained for the fluid located at the top or bottom of the structure. In general, for those variables at the exterior sides of the Eulerian cell which cannot be computed by the conservation equations, extrapolation of their values from the interior region is necessary. The velocity components can be obtained from the mass conservation equation. These multi-valued velocity fields will be used consistently in the particle-movement and source-term modification. They are also utilized in handling fluid motion at the geometrical discontinuity. For further details, see ref. [7].

2.4 Finite-element Structural Program

The responses of the components of the containment structures such as the radial shield, the core barrel, the core-support structure, and the primary vessel are analyzed by a well-developed finite-element program, WHAM [5]. This program employs a convected-coordinates scheme in the numerical analysis and is best suited for large-displacement, small-strain, elastic-plastic, dynamic problems. In this scheme, convected coordinates of the element rotate, but do not deform with the elements. The strain is linearly related to the displacement of the element relative to the convected coordinates. Similarly, the nodal forces are linearly related to element stresses. At the present time, the program has conical-shell and axisymmetric triangular continuum elements which can be used to simulate the complicated structure components.

2.5 Simultaneous Iteration Scheme

Because the source term of the relaxation equation at the fluid-structure interface is proportional to the mass flux, the pressure, density, and velocity fields must be iterated simultaneously. Thus, after each iterate giving the pressure field, the density and velocity fields are immediately computed by the equation of state and the momentum equations, respectively. Based upon the new density and velocity, the mass flux at the interface is appropriately adjusted, which results in a new pressure in the boundary cell. This procedure is repeated until the boundary conditions at all interfaces are rigorously satisfied. In other words, for the deformable structure without openings (i.e., $\theta_{k,\ell} = 0$ in eq. (3)), the iteration is continued until the fluid slides tangentially. For the perforated structures, on the other hand, the procedure is repeated until the uniform mass flux across the boundary equals to the total mass flux through the openings.

3. Sample Problems

3.1 Responses of Components and Containment to Low-energy Excursion

The first investigation studies the response of a typical LMFBR primary containment to an HCDA. The mathematical model, shown in Fig. 2, consists of a reactor core, coolant, radial shield, core barrel, core-support structure, and the primary vessel. Since the shield material does not have tensile strength in the circumferential direction, it is considered as a compressible fluid with the same mass and compressibility as the actual material. The core-support structure is modeled as a composite structure made of plates and shells as for the actual structure. To simplify the analysis, the openings in the core-support structure are not included in the model. Thus, the transmission of pressure pulses into the lower plenum depends solely on the downward motion of the core-support structure. The energy release in the reactor core was characterized by a pressure-volume relationship, which has an initial pressure of 20.4 MPa and decays exponentially.

Figure 3 presents the reactor configurations at three different times. These configurations show the expansion of the core-gas bubble, the motion of the coolant, and the responses

of the core barrel, the core-support structure, and the primary vessel. They also show that the fluids slide along all the internal interfaces during the course of the motion. Note that fluids on both sides of the core barrel exhibit different motion. At the left-hand side, the fluid moves upward in the radial shield; at the right-hand side, the fluid remains relatively undisturbed. Moreover, certain strong disturbances of the fluid motion occur at the upper end of the core barrel during the later stage of excursion, which is believed to be induced by the vibration of the core barrel.

To illustrate the response of the containment structure, the axial displacements at the center of the core-support structure and the center of the primary vessel are given in Fig. 4. Due to large pressure gradient between the upper and lower plenums at the initial stage of excursion, these structures are displaced downward and gradually attain their maximum displacement. However, at the later stage of the excursion, the pressure in the upper plenum becomes small, which in turn causes the structures to be displaced upward.

The radial displacements of the shield material and core barrel (see nodes A and B in Fig. 2) opposite the core are shown in Fig. 5. Due to the strong outward pressure gradient the peak displacements are found at 6 ms. Thereafter, the pressure between the barrel and the primary vessel gradually builds up and thus causes the displacements to decrease. The peak displacement of the shield material is greater than that of the core barrel. This is because the radial shield is treated as compressible fluid which has less rigidity than the core barrel.

3.2 The Effect of Core-support Structure (CSS) Openings on the Pressure Loading in the Reactor Lower Plenum

In the first example, we did not take into consideration the sodium flow through the coolant passage openings. Although the solution gives conservative results for the slug impact and the upper vessel deformation, it underestimates the pressure loading at the inlet-nozzle region. In order to understand the influence of the CSS openings on the wave motion in the reactor plenum, we present here an analysis which accounts for the coolant flow through CSS openings, and compare the results concerning the pressure loadings and bottom-vessel deformations for the cases with and without openings in the CSS.

The reactor configuration chosen for the analysis is the same as used in the previous example. In the calculation, we assume that the flow areas associated with each radial structure member is different from one another, and that the perforation ratio of this area to its total area is given in Table 1.

Because of the presence of the openings in the CSS immediately below the core region, fluids thus can penetrate and separate at the boundaries. This is evident from Fig. 6, which gives the reactor configurations at three different times. From these configurations one can see how the fluids flow across the CSS in the upper plenum and how the fluids flow away from the boundary due to fluid jetting in the reactor lower plenum. They also show that, at other structure members without perforated openings, the fluids do slide along the solid boundaries during the motion.

Figure 7 shows the pressure loadings in the reactor lower plenum for the cases with and without openings. Figure 8 presents the axial deformation of the bottom vessel. Obviously, if the openings of the CSS are not considered, the pressure loading in the reactor lower plenum and the axial deformation of reactor bottom are underestimated. The degree of the underestimation is, of course, dependent on the perforation ratio of the core-support structure.

The total forces on the reactor cover obtained from these two cases are also compared. As we anticipate, the results reveal that the peak force is larger when there are no openings than when openings occur. However, the difference is very small.

4. Conclusions

The Eulerian algorithm described here is capable of analyzing two-dimensionally the fluid-structure interaction in a typical LMFBR containment consisting of various structure components. The algorithm has several special features. First, it employs the Eulerian coordinates in the formulation and enables the technique to be applicable to excursions involving large material distortions. Second, it provides rigorous hydrodynamic analyses at the fluid-structure interface and at the geometrical discontinuities, which is very important in the study of wave-transmission and -diffraction problems. Third, the algorithm incorporates a well-developed finite-element structural program that can account for both material and geometrical nonlinearities.

The application of this Eulerian algorithm is not limited to fast reactor containment. It can also be applied to the major piping components, such as valve and IHX, where internal baffle plates may play an important role in the wave propagation. Moreover, the treatment of the time-dependent irregular cell can be integrated with the IMF^2 Method and structural dynamics program for investigating the coupled fluid-structure problems involving two-phase flows.

5. Acknowledgements

The authors would like to express grateful appreciation to D. Basinger and B. J. Hsieh for their assistance in the modification of the structural program.

The work described in this paper was done in the Engineering Mechanics Section of Reactor Analysis and Safety Division, and was performed under the auspices of the Energy Research and Development Administration.

References

[1] HARLOW, F. H. and AMSDEN, A. A., "A Numerical Fluid Dynamics Calculation Method for all Flow Speed," J. Comp. Phys., 8, p.197 (1971).

[2] HARLOW, F. H. and AMSDEN, A. A., "Flow of Interpenetrating Material Phases," J. Comp.Phys., 18, p.440 (1975).

[3] WANG, C. Y., An Implicit Eulerian Method for Calculating Fluid Transients in Fast Reactor Containment, USERDA Rep. ANL-75-81, Argonne National Laboratory (1975).

[4] WANG, C. Y., CHU, H. Y., CHANG, Y. W., and FISTEDIS, S. H., "Application of the Implicit Eulerian Method (ICECO) to Fast Reactor Containment," Third Intl. Conf. on Structural Mechanics in Reactor Technology, London, Sept. 1-5, 1975, paper E 3/4, vol. 2E.

[5] BELYTSCHKO, T. and HSIEH, B. J., "Nonlinear Transient Analysis of Shells and Solids of Revolution by Convected Coordinates," AIAA Vol. 12, No. 8., p.1031 (1974)

[6] SCHLICHTING, H., "Boundary-Layer Theory," McGraw-Hill Book Co., New York, N. Y. (1969).

[7] WANG, C. Y., A Generalized Eulerian Method for Analyzing Nonlinear Fluid-structure interaction in the Primary Containment, Argonne National Laboratory report (to be published).

Table 1

Perforation Ratio of the Core-Support Structure

Radial Zone for the Corresponding Member	Perforation Ratio
2	0.15
3	0.10
4	0.05
5 - 9	0

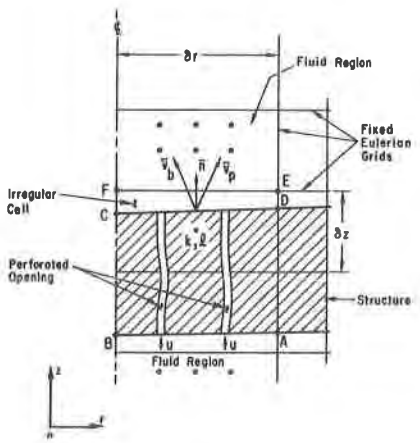

Figure 1. Irregular Cell (k,ℓ) Containing Deformable Structure

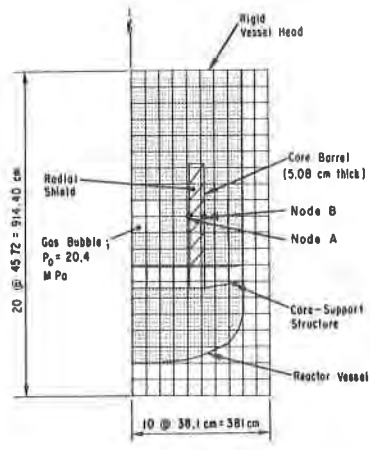

Figure 2. Initial Configuration used in the Analysis

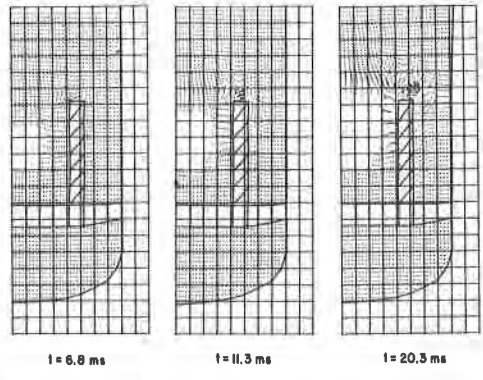

Figure 3. Configurations at Various Times

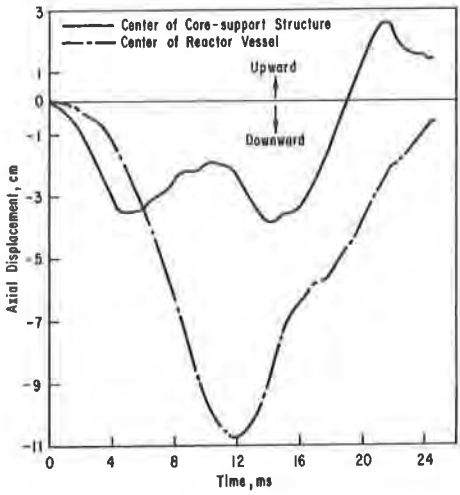

Figure 4. Calculated Axial Displacements As a Function of Time

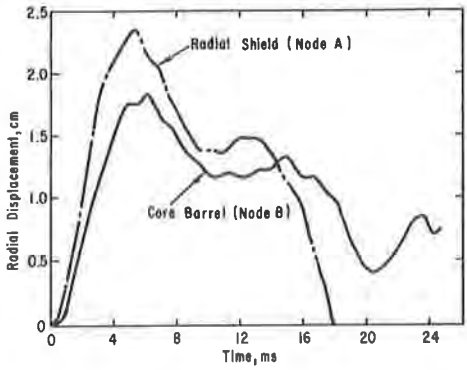

Figure 5. Calculated Radial Displacements As a Function of Time

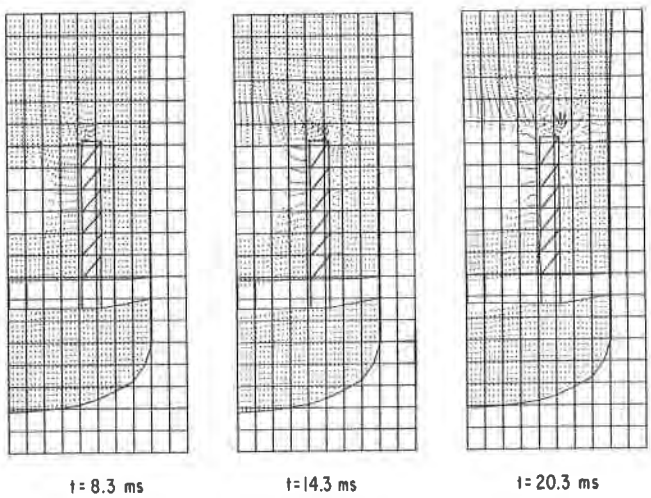

Figure 6. Reactor Configurations at Three Different Times

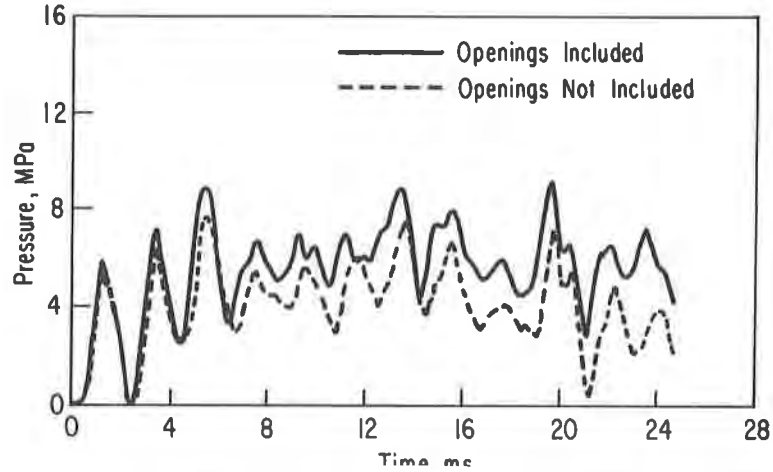

Figure 7. Pressure Loadings in the Reactor Lower Plenum

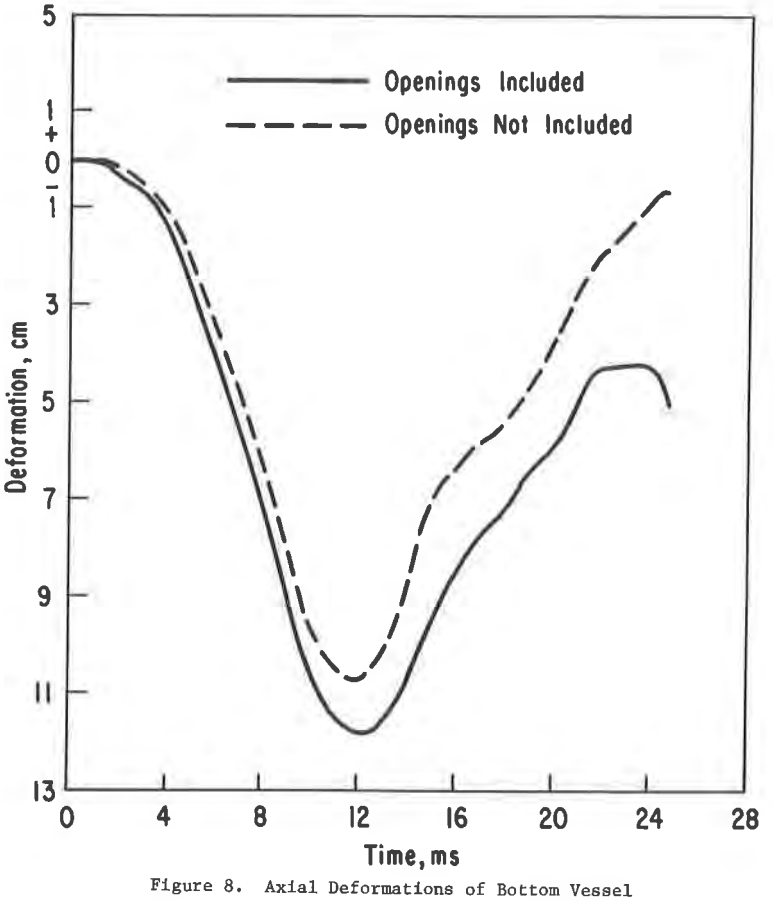

Figure 8. Axial Deformations of Bottom Vessel